Journal of Hydrology 540 (2016) 162–175

Contents lists available at ScienceDirect

Journal of Hydrology

journal homepage: www.elsevier.com/locate/jhydrol

Effect of DOC on evaporation from small Wisconsin lakes

C.J. Watras *, K.A. Morrison, J.L. Rubsam

Fishery and Aquatic Science Section, Wisconsin Department of Natural Resources, Madison, WI 53707, USA
Center for Limnology, University of Wisconsin-Madison, Trout Lake Station, 3110 Trout Lake Station Dr., Boulder Junction, WI 54512, USA

ARTICLE INFO

Article history:
Received 19 January 2016
Received in revised form 23 May 2016
Accepted 1 June 2016
Available online 6 June 2016
This manuscript was handled by Tim R. McVicar, Editor-in-Chief

Keywords:
Evaporation
Dissolved organic carbon
Wind-sheltered lakes
Floating evaporation pans
Mass transfer models

SUMMARY

Evaporation (E) dominates the loss of water from many small lakes, and the balance between precipitation and evaporation (P–E) often governs water levels. In this study, evaporation rates were estimated for three small Wisconsin lakes over several years using 30-min data from floating evaporation pans (E-pans). Measured E was then compared to the output of mass transfer models driven by local conditions over daily time scales. The three lakes were chosen to span a range of dissolved organic carbon (DOC) concentrations (3–20 mg L^{-1}), a solute that imparts a dark, tea-stain color which absorbs solar energy and limits light penetration. Since the lakes were otherwise similar, we hypothesized that a DOC-mediated increase in surface water temperature would translate directly to higher rates of evaporation thereby informing climate response models. Our results confirmed a DOC effect on surface water temperature, but that effect did not translate to enhanced evaporation. Instead the opposite was observed: evaporation rates decreased as DOC increased. Ancillary data and prior studies suggest two explanatory mechanisms: (1) disproportionately greater radiant energy outflux from high DOC lakes, and (2) the combined effect of wind speed (W) and the vapor pressure gradient ($e_s - e_z$), whose product [$W(e_s - e_z)$] was lowest on the high DOC lake, despite very low wind speeds (<1.5 m s^{-1}) and steep forested uplands surrounding all three lakes. Agreement between measured (E-pan) and modeled evaporation rates was reasonably good, based on linear regression results (r^2: 0.6–0.7; slope: 0.5–0.7, for the best model). Rankings based on E were similar whether determined by measured or modeled criteria (high DOC < low DOC). Across the 3 lakes and 4 years, E averaged ~3 mm d^{-1} (C.V. 9%), but statistically significant differences between lakes resulted in substantial differences in cumulative E that were consistent from year to year. Daily water budgets for these lakes show that inputs were dominated by P and outputs by E; and our findings indicate that subtle changes in the variables that drive E can have measurable effects on water levels by shifting the balance between P and E.

1. Introduction

Evaporation (E) and precipitation (P) govern the global water cycle, with continental runoff (Q) being reconciled by excess evaporation from the oceans (Brutseart, 1982). On regional scales, the balance between P and E defines climate. In humid regions, the quantity (P–E) is relatively large, and aridity increases as (P–E) decreases. Recent studies in the humid upper Great Lakes region of North America indicate that inter-annual changes in (P–E) have driven a near-decadal oscillation of water levels in lakes and aquifers for most of the last century (Watras et al., 2014a). Related studies by Hanrahan et al. (2010, 2014) suggest that a recent downward trend in this water level time series has been driven by accelerating evaporation. Mechanistic explanations include declines in the duration of ice-cover (Magnuson et al., 2000), increases in summertime water temperature (Austin and Colman, 2007; Hanrahan et al., 2010; Mishra et al., 2011; O'Reilly et al., 2015) and solar forcing associated with atmospheric brightening due to reductions in anthropogenic aerosols like sulfate (Wild and Liepert, 2010; Wild, 2012).

Under a warming earth scenario, both P and E would be expected to accelerate globally; but one argument holds that E would increase faster than P over land leading to a dryer future in many regions (Sherwood and Fu, 2014). This argument posits that land surfaces will warm faster than the ocean; and consequently, the vapor pressure deficit over land will increase more than other hydrologic quantities yielding higher E relative to P and expanded aridity, on average. A trend toward expanded aridity is not inconsistent with future climate scenarios projecting more rainfall provided there are also longer intervening periods

* Corresponding author at: Trout Lake Research Station, 3110 Trout Lake Station Drive, Boulder Junction, WI 53707, USA.
E-mail address: cjwatras@wisc.edu (C.J. Watras).

http://dx.doi.org/10.1016/j.jhydrol.2016.06.002
0022-1694/

of dryout between precipitation events (Melillo et al., 2014). However, at least two alternative hypotheses argue against the general expansion of aridity over land: (1) Held and Soden (2006) argue that the "wet will get wetter, and the dry will get drier," based on zonal (latitudinal) modeling; and (2) Roderick et al. (2014) argue that the future warming of land will result in disproportionately more radiative outflux (long-wave) and, consequently, smaller increases in E relative to P. Since surface temperate is not the only climatic variable likely to shift in a warmer future, changes in near-surface wind speed (W) could also be an important factor driving E, especially in humid regions (McVicar et al., 2012).

At local scales, changing levels of surface waters and aquifers have important social, economic and ecological implications. However, our ability to relate observational data to the balance between P and E is limited by sparse information on evaporation. Although precipitation is routinely measured with relatively high accuracy and spatial resolution across many regions, measurements of evaporation from water surfaces are less common. Where available, estimates of E from surface waters are usually based on water balance, energy balance, eddy covariance or mass transfer models. A large number of model formulations have been proposed, and the choice of an appropriate modeling approach often entails a trade-off between cost and accuracy (Rosenberry et al., 2007).

As an alternative or complement to modeling approaches, evaporation can be measured directly using evaporation pans (E-pans) that are partially submerged in a water body (Masoner et al., 2008; Masoner and Stannard, 2010; Mendoza-Sanchez et al., 2013). Floating E-pans avoid some of the concerns associated with E-pan deployment in water limited settings (Brutsaert and Parlange, 1998), and they simulate site-specific conditions at the water surface (turbulence, heat storage, heat transfer, surface temperature and vapor pressure). They also simplify computation. In a floating E-pan, the water balance has just two terms: $\Delta S = E$, where S is the stage or water level in the pan after precipitation inputs are subtracted. Although the turbulent diffusion of heat can be underrepresented in very shallow E-pans, and although current designs are limited to low-fetch waters, floating E-pans configured with fast, high-precision water level sensors enable the direct determination of E over a wide range of ambient conditions and time scales (sub-hourly to years). As such, floating E-pans provide independent measures of E that enable the refinement of models in natural settings.

In this study, we compare direct and indirect estimates of evaporation from three small Wisconsin lakes over sub-hourly to interannual time scales. The direct measurements were made using floating evaporation pans with differential pressure sensors that recorded water levels at 30 min time intervals with an operational

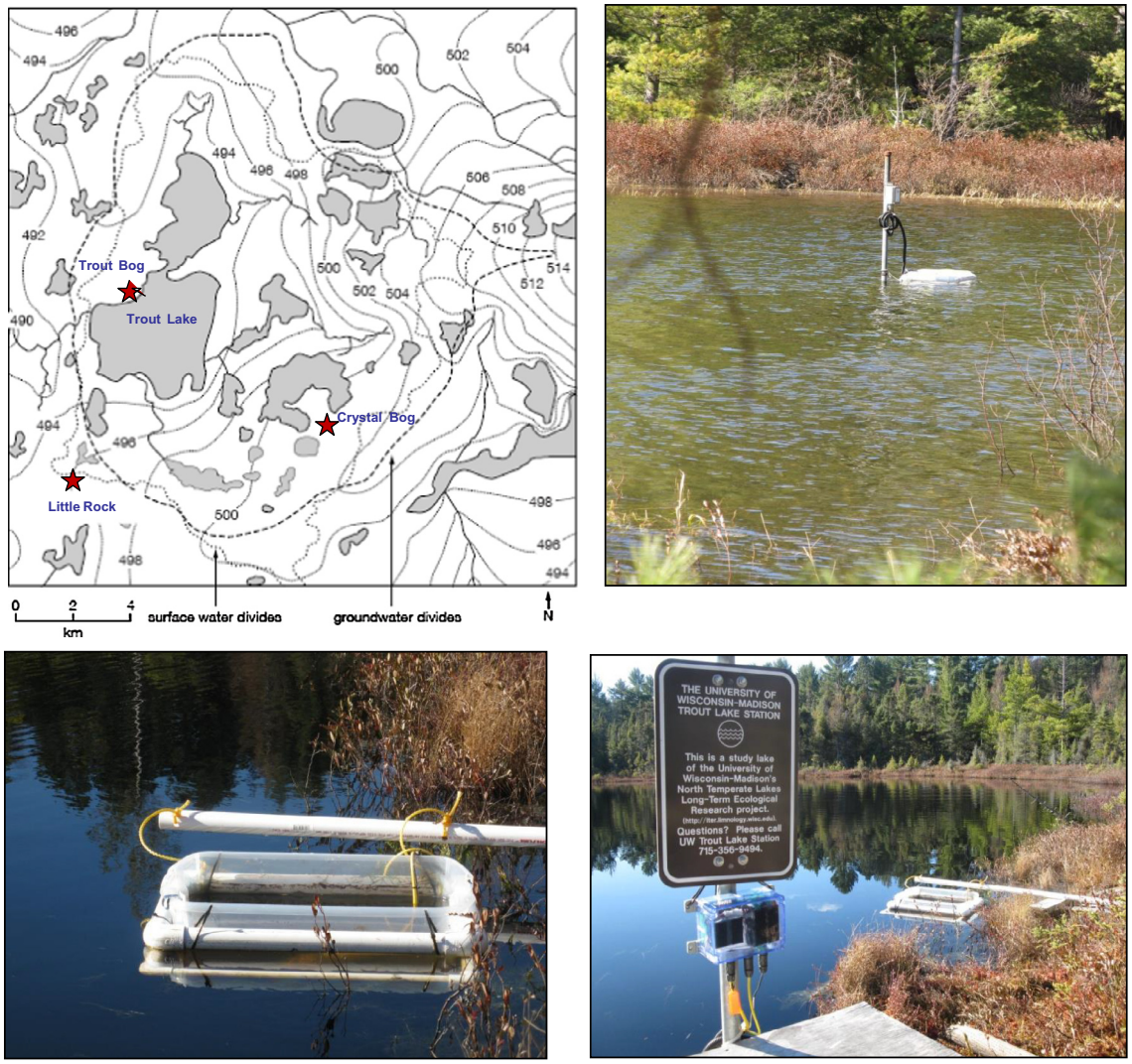

Fig. 1. Map of study area and deployment of evaporation pans with radio sensors in Little Rock Lake (upper right), Trout Bog (lower left) and Crystal Bog (lower right).

Table 1
Limnological characteristics of the three study lakes in northern Wisconsin (https://lter.limnology.wisc.edu/about/lakes). Spectral slopes ($S_{275-295}$) see Fig. 2 and Helms et al. (2008).

	Trout Bog	Crystal Bog	Little Rock Lake
Latitude	46.041	46.008	45.996
Longitude	−89.686	−89.606	−89.706
Area (ha)	1	0.6	17.9
Depth, maximum (m)	7.9	2.5	10.3
pH	4.8	5.2	6.1
ANC (μeq L^{-1})	11	14	31.5
DOC (mg L^{-1})	19.9	10.6	3.2
Conductivity (μS cm^{-1})	23	11	12
TN (μg L^{-1})	961	722	312
TP (μg L^{-1})	46.6	18.2	8.3
$S_{275-295}$ (nm^{-1})	0.0139	0.0135	0.0178

resolution and precision of 0.1 mm H_2O. Indirect estimates of E were made simultaneously using three mass transfer models supported by high-frequency measurements of near-surface water temperature, air temperature, relative humidity, barometric pressure and wind speed. The study lakes were selected to span a wide range of dissolved organic matter (humic DOC, 3–20 mg C L^{-1}), a ubiquitous solute whose optical properties enhance the absorbance of the solar radiation that ultimately drives evaporation.

Assuming that higher light absorbance would result in higher near-surface water temperatures (T_s), and given that the vapor pressure of water increases exponentially with T_s, we initially hypothesized that large differences in DOC would manifest as significant differences in E, all other things being equal. To isolate and quantify a DOC effect, we focused on small, wind-sheltered seepage lakes that minimize variability due to fetch and tributary flows. Such lakes are common in northern Wisconsin, and they are often dominant features of the landscape at mid- and high latitudes (Downing et al., 2006; McDonald et al., 2012). Our main objectives were: (1) to investigate whether DOC modulates evaporation in a predictable way, (2) to evaluate correlations between measured E and climatic variables at various time scales (sub-hourly, daily, weekly, monthly), (3) to compare measured E to modeled E using several mass transfer models, and (4) to construct high frequency water budgets using directly measured E, P and S (lake stage), all determined at 30 min time intervals for the open water period.

2. Methods

2.1. Study sites

The three study lakes are situated within the Trout Lake watershed, a 130 km^2 forested catchment nested within the Northern Highland Lake District (NHLD) of northern Wisconsin (Fig. 1). The catchment contains roughly 115 lakes and ponds which range in size from 200 m^2 to 15 km^2 and have a combined surface area of 30 km^2 (Magnuson et al., 2006). The local geology consists of thick till and outwash sands (30–60 m) deposited during the Wisconsin glacial retreat 10ky BP (Attig, 1985). All three lakes are seepage systems with no inflowing or outflowing streams.

The Trout Bog sub-catchment comprises a heavily forested peatland (4.5 ha) surrounding a 1 ha bog pond. The Crystal Bog sub-catchment comprises a larger, more sparsely forested peatland (7 ha) surrounding a 0.6 ha bog pond. The Little Rock Lake sub-catchment contains very little riparian peatland, and as a result the lake water is relatively clear. All three lakes are sheltered by steeply sloping uplands containing mature stands of oak and pine. The shorelines are undeveloped and the lakes are relatively pristine. Limnological characteristics are summarized in Table 1.

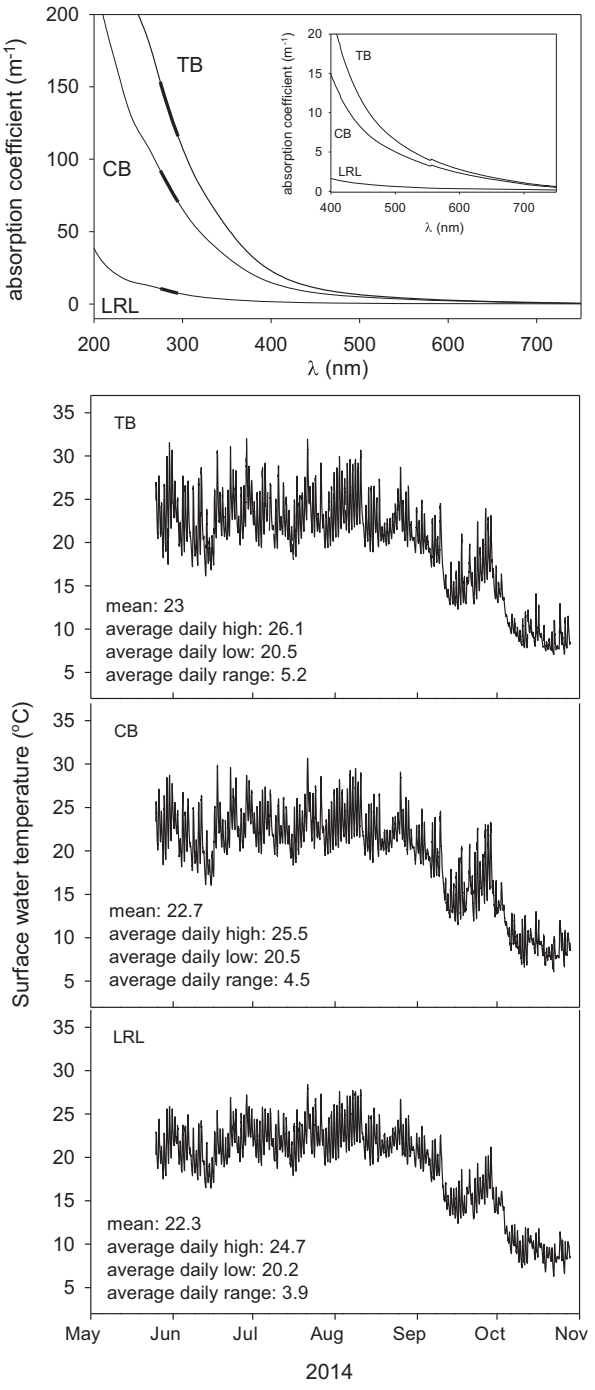

Fig. 2. Light absorbance and temperature in surface waters of the three study lakes in 2014. TB, Trout Bog; CB, Crystal Bog; LRL, Little Rock Lake. Darkened segment in top panel is the region where the spectral slope coefficient was calculated (Table 1). Insert expands PAR region. Means, highs, lows and ranges calculated for 30 min data for the mid-summer time period: 1 July 31 to August.

2.2. Evaporation pans and water level measurement

Evaporation was measured with floating E-pans that consist of a clear plastic box (40 cm wide × 35 cm deep × 50 cm long) with thin walls (~2 mm) to facilitate thermal equilibration with the ambient lake water (Fig. 1; Suppl. Fig. 3). Each pan was filled with lake water and outfitted with a floatation collar so that the top was elevated a few cm above the surface of the lake. Water levels inside and outside the box were adjusted manually to be similar. The evaporation pans were manually tended each week to

Table 2
Differences in surface water temperature among the study lakes using 30 min data for the full study period each year (paired *t*-tests, *p* is the probability that the mean difference between temperatures is significant at $\alpha = 0.05$). CI, confidence interval. TB, Trout Bog; CB, Crystal Bog; LRL, Little Rock Lake. Conclusion: TB > CB > LRL, all years.

Year	Lake Pair	Surface water temperature	
		Mean difference °C (95% CI)	*p*
2015	TB–CB	0.56 (0.012)	<0.001
	CB–LRL	0.10 (0.024)	<0.001
	TB–LRL	0.67 (0.029)	<0.001
2014	TB–CB	0.24 (0.015)	<0.001
	CB–LRL	0.40 (0.021)	<0.001
	TB–LRL	0.67 (0.023)	<0.001
2013	TB–CB	0.24 (0.016)	<0.001
2012	TB–CB	0.31 (0.015)	<0.001

Table 3
Differences in daily evaporation rates among the study lakes (paired *t*-tests, *p* is the probability at $\alpha = 0.05$). Time spans: 2015: 17 May to 10 November ($n = 178$ d); 2014: 26 May to 29 October ($n = 157$ d); 2013: 11 May to 31 October ($n = 174$ d). Model is Ryan–Harleman (Eq. (3)). TB, Trout Bog; CB, Crystal Bog; LRL, Little Rock Lake. Conclusion: LRL > CB > TB.

Year	Lake Pair	Measured evaporation		Modeled evaporation	
		Mean difference (mm d^{-1})	*p*	Mean difference (mm d^{-1})	*p*
2015	LRL–TB	0.91	<0.001	NA[a]	NA
	CB–TB	0.69	<0.001	NA	NA
	LRL–CB	0.23	<0.01	NA	NA
2014	LRL–TB	0.39	<0.001	0.15	<0.001
	CB–TB	0.20	<0.001	0.40	<0.001
	LRL–CB	0.18	0.05	−0.25	<0.001
2013	CB–TB	0.41	<0.001	0.42	<0.001

[a] NA: no estimate because meteorological data unavailable in 2015.

compensate for evaporative losses and rainfall inputs. There were 1 mm graduations in each pan so that the water level could be re-adjusted each week to the starting height. The E-pans were deployed soon after ice-off in the spring and maintained until the first snowfall in late autumn each year.

A differential pressure sensor that was temperature compensated and vented to the atmosphere was mounted in each E-pan to track the water level at 30 min time intervals (PT2X Smart Sensor, Instrumentation Northwest, Inc.). Each PT2X sensor logged water level and temperature data internally. The sensor and logger were interfaced with a radio frequency modem that operated on the 900 MHz band. The sensors and data loggers were powered by 2 AA batteries (3 V), and the radios were powered by 8 AA batteries (12 V). The logged data were accessed periodically by wireless RF communication via a transceiver interfaced with a hand-held laptop computer on shore. Additional details on the sensing and communication protocols can be found in Watras et al. (2014b).

2.3. Data quality

The nominal accuracy and resolution of the thermally and barometrically compensated (vented) PT2X pressure sensors were

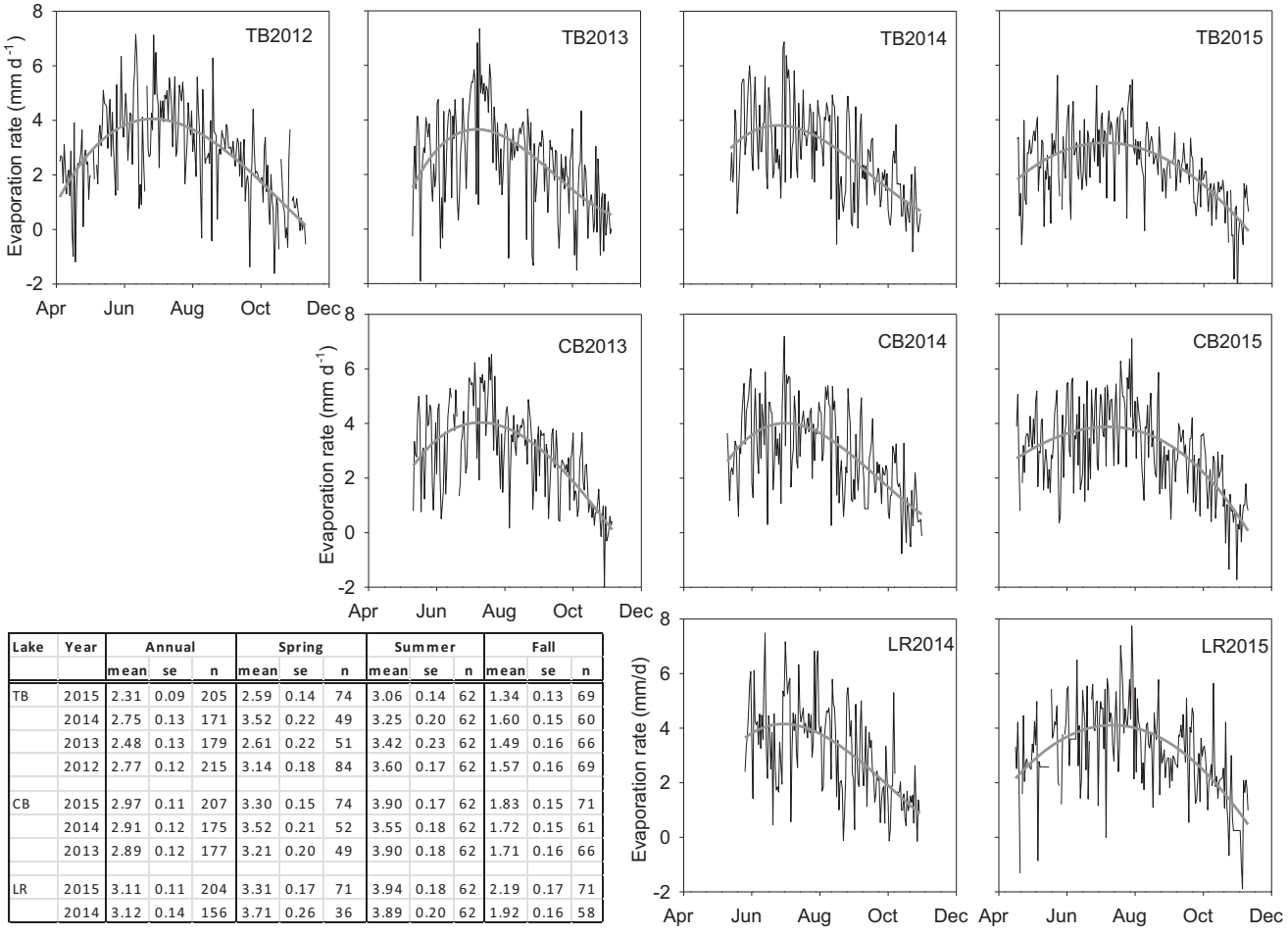

Lake	Year	Annual			Spring			Summer			Fall		
		mean	se	n	mean	se	n	mean	se	n	mean	se	n
TB	2015	2.31	0.09	205	2.59	0.14	74	3.06	0.14	62	1.34	0.13	69
	2014	2.75	0.13	171	3.52	0.22	49	3.25	0.20	62	1.60	0.15	60
	2013	2.48	0.13	179	2.61	0.22	51	3.42	0.23	62	1.49	0.16	66
	2012	2.77	0.12	215	3.14	0.18	84	3.60	0.17	62	1.57	0.16	69
CB	2015	2.97	0.11	207	3.30	0.15	74	3.90	0.17	62	1.83	0.15	71
	2014	2.91	0.12	175	3.52	0.21	52	3.55	0.18	62	1.72	0.15	61
	2013	2.89	0.12	177	3.21	0.20	49	3.90	0.18	62	1.71	0.16	66
LR	2015	3.11	0.11	204	3.31	0.17	71	3.94	0.18	62	2.19	0.17	71
	2014	3.12	0.14	156	3.71	0.26	36	3.89	0.20	62	1.92	0.16	58

Fig. 3. Daily evaporation rates measured in floating E-pans for all lakes and years. Curves indicate the seasonal cycle (cubic fit). Tabulated data are mean, standard error (se) in mm d^{-1} and number of days with measured rates (n). Seasons are: starting date through June (spring), July and August (summer), September and October (fall).

±0.06% FSO and 16 bit, respectively (Instrumentation Northwest, Inc.). Since the measurement range of the sensor was 5 psig, the nominal water depth accuracy and resolution were 2.1 mm and 0.05 mm (i.e. 3515 mm $H_2O/2^{\wedge 16}$), respectively. Accuracy was determined relative to standardized dead weight pressures of 0.000 psi, 2.500 psi and 5.000 psi, and sensor precision was determined by repeated measurements against a single pressure. Results indicated repeatability to within 0.1 mmH_2O, and that value was considered the limit of operational precision and resolution. Each PT2X sensor was also temperature compensated by INW under constant pressure along a series of temperatures from 0 °C to 40 °C. A second order polynomial fit to the calibration data was integrated into the sensor firmware (INW Inc., 1995). Further details and technical specifications of the PT2X sensors are available from INW, Kent, Washington, USA.

2.4. Data processing

The raw 30-min water level data were first corrected for precipitation and manual adjustments. Noise was reduced by applying a 3.5 h centered running mean to the corrected water level data, and evaporation rates were estimated as E = ΔS for each 30 min time step. Daily evaporation was calculated as the sum of 48 estimates of E per day. Evaporation rates for days with missing data were estimated by linear interpolation of the daily time series. Our criterion for identifying outliers was ±3 standard deviations from the mean daily E after removing the seasonal cycle. Across the full data set of 1701 daily observations, there were 17 d with missing data (1%) and 12 outliers (0.7%). Data processing was performed using Matlab R2014b. Graphical and statistical analyses were performed using SigmaPlot 13 and AutoSignal 1.7.

2.5. Mass transfer models

As summarized by Adams et al. (1990) and Rasmussen et al. (1995), the evaporation of liquid water can result from (1) forced convection due to the horizontal movement of air across the water surface, and/or (2) free convection due to the density difference between air at the water surface and air higher up (i.e. water saturated air is more buoyant than dryer air at the same temperature). Mass transfer models capture these two processes in various ways, and they express evaporative loss in terms of either an energy flux rate (W m^{-2}) or a water flux rate (mm d^{-1}).

Ryan et al. (1974) modeled evaporative loss due to free convection as:

$$\phi_e = \lambda(T_{sv} - T_{az})^{1/3}(e_s - e_z) \quad (1)$$

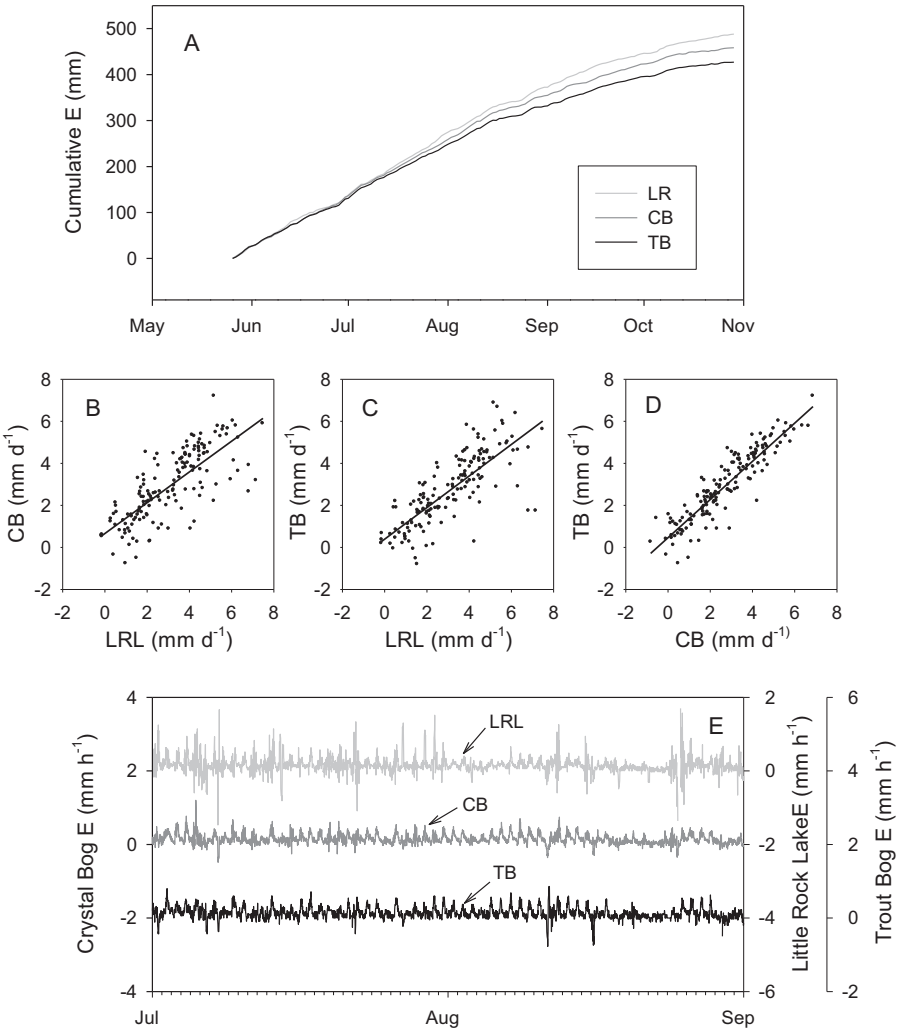

Fig. 4. Measured rates of evaporation during 2014. LRL: Little Rock Lake; CB: Crystal Bog; TB: Trout Bog. In panel A, cumulative E is the running sum of daily E, including all positive and negative values. Correlations (r^2) in B, C, and D are 0.58; 0.61; 0.83, respectively (n = 157 d). Time series in E are the 3.5 h centered moving average of the 30 min data.

where

ϕ_e = evaporative heat loss (W m^{-2})

$\lambda = 2.7$ W/m^2 hPa(°C)$^{1/3}$

T_{sv} = virtual temperature of saturated air at temperature of surface water (°C)

T_{az} = virtual temperature of air at height z (°C)

e_s = saturation vapor pressure of water at water surface temperature (hPa)

e_z = water vapor pressure in air at height z (hPa).

The quantities $(T_{sv} - T_{az})$ and $(e_s - e_z)$ are the virtual temperature gradient and the vapor pressure gradient, respectively. Virtual temperature is the temperature that dry air would be when at equivalent density as the wetted air, estimated as $T_v(\mathrm{K}) = T(\mathrm{K})(1.061{\cdot}\omega)$ where ω is the mixing ratio $(0.62197{\cdot}e/(\rho - e))$, e is vapor pressure (hPa) and ρ is air pressure (hPa). As indicated in Eq. (1), evaporative loss is directly related to the vapor pressure deficit, while the effect of the virtual temperature difference is nonlinear.

As described by Brutseart (1982), an early revision of the original Dalton evaporation model added a wind function to include forced convection as:

$$\phi_e = (a + bW_z)(e_s - e_z) \quad (2)$$

where a and b are fitted constants and W_z is the wind speed at height z.

Ryan and Harleman (1973) substituted $a = (\phi_e)_{free}$ as in Eq. (1) and left b as the constant 3.1 in their model:

$$\phi_e = [\lambda(T_{sv} - T_{az})^{1/3} + 3.1W_z](e_s - e_z) \quad (3)$$

Adams and Helfrich (1982) combined free and forced convection as the square root of the sum of squares, such that $\phi_e = \left[\phi^2_{free} + \phi^2_{forced}\right]^{1/2}$. They derived Eq. (4) using Eq. (1) to represent free convection and using a fetch-dependent model from Harbeck (1962) to represent forced convection yielding:

$$\phi_e = \left\{[\lambda(T_{sv} - T_{az})^{1/3}]^2 + [5.1A^{-0.05}W_2]^2\right\}^{1/2}(e_s - e_z) \quad (4)$$

where A is the surface area of the water body.

We used site-specific ancillary data as inputs to these models, and we used linear regression to compare their output to the measured rates of evaporation from floating E-pans. Energy flux rates (W m^{-2}) were converted to water flux rates (mm time^{-1}) using the volumetric latent heat of vaporization (joules volume^{-1}).

2.6. Ancillary data

Precipitation was monitored on site using NovaLynx 260–2500 tipping rain gauges (calibration: 0.25 mm; accuracy: ±0.5 mm at 5 cm h^{-1}) with data loggers. High-frequency measurements (1 min) of near-surface water temperature (NexSens TS110-C, 0.1 m depth), air temperature and relative humidity (Campbell Scientific HMP50-L, 1 m above water surface), and wind speed (RM Young 03301 Wind Sentry, 2 m above water surface) were made from rafts on Trout Bog and Crystal Bog. Incoming solar radiation and barometric pressure were measured each minute at a single nearby location (45.93, −89.73) with an Eppley PSP pyranometer and a Vaisala WXT500 weather station, respectively. The one minute data were averaged over 30 min time intervals to be consistent with the frequency of E-pan measurements. For Little Rock Lake, we used meteorological data from nearby Sparkling Lake (~300 m to the north) and Crystal Bog for modeling purposes.

In addition to micro-meteorological data, lake stage was recorded in Crystal Bog and Trout Bog using stilling wells with PT2X sensors that logged data at 30 min time intervals to be consistent with the climatic data (Watras et al., 2014b). Lake stage was referenced to an arbitrary benchmark at both sites. Along with simultaneous precipitation and evaporation data, the stage data allowed us to construct daily water budgets wherein net seepage was estimated as a residual term.

Light absorption spectra for water from each lake were determined with a Beckman Coulter DU800 spectrophotometer with quartz cells over the wavelength range 200–750 nm. The spectral slope coefficient ($S_{275-295}$) was calculated as an indicator of DOC composition and source (Helms et al., 2008). Diffuse light attenuation coefficients (Kd, m^{-1}) and their relation to DOC were obtained from the literature (Williamson et al., 1996; Read and Rose, 2013).

Table 4
Pearson correlations (r) between measured rates of evaporation and climate variables across years, lakes and time-scales. TB, Trout Bog; CB, Crystal Bog; LRL, Little Rock Lake. $(e_{sw} - e_a)$, vapor pressure deficit; SSR, shortwave solar radiation; Tw, water temperature; Ta, air temperature; RH, relative humidity; (Tvs–Tva)$^{1/3}$ virtual temperature difference (cube root); Bar, barometric pressure; W, wind speed.

Year	Lake	Timeframe	$(e_{sw} - e_a)$	SSR	Tw	Ta	RH	(Tvs–Tva)$^{1/3}$	Bar	W
2014	TB	30 min	0.55	0.51	0.35	0.36	−0.55	0.02	0.12	0.34
		Daily	0.86	0.87	0.56	0.43	−0.69	0.44	0.24	0.18
		Week	0.93	0.94	0.76	0.69	−0.65	0.73	0.27	0.12
		Month	0.97	0.98	0.85	0.85	−0.60	0.88	0.39	−0.15
	CB	30 min	0.59	0.52	0.39	0.40	−0.55	−0.01	0.14	0.31
		Daily	0.88	0.86	0.63	0.48	−0.67	0.39	0.25	−0.03
		Week	0.95	0.92	0.77	0.70	−0.57	0.68	0.30	0.03
		Month	0.99	0.96	0.92	0.92	−0.46	0.85	0.45	−0.01
	LRL	30 min	0.24	0.17	0.14	0.12	−0.19	0.02	0.02	0.13
		Daily	0.35	0.27	0.22	0.12	−0.16	0.22	0.06	0.07
		Week	0.91	0.88	0.72	0.63	−0.58	0.63	0.28	0.10
		Month	0.95	0.96	0.87	0.90	−0.63	0.34	0.47	−0.16
2013	TB	30 min	0.55	0.45	0.35	0.35	−0.54	0.04	0.12	0.32
		Daily	0.82	0.81	0.57	0.43	−0.63	0.34	0.29	0.25
		Week	0.93	0.91	0.84	0.80	−0.58	0.51	0.42	−0.14
		Month	0.99	0.94	0.95	0.94	−0.81	0.96	0.66	0.42
	CB	30 min	0.60	0.46	0.40	0.40	−0.56	0.00	0.14	0.34
		Daily	0.87	0.88	0.63	0.47	−0.66	0.34	0.30	0.20
		Week	0.97	0.93	0.89	0.85	−0.56	0.52	0.41	0.08
		Month	0.99	0.97	0.96	0.96	−0.76	0.94	0.67	0.22
2012	TB	30 min	0.25	0.13	0.17	0.16	−0.20	0.01	0.04	0.10
		Daily	0.71	0.67	0.51	0.43	−0.53	0.30	0.17	0.14
		Week	0.91	0.86	0.84	0.82	−0.44	0.45	0.13	−0.24
		Month	0.97	0.92	0.97	0.97	−0.47	0.52	−0.30	−0.39

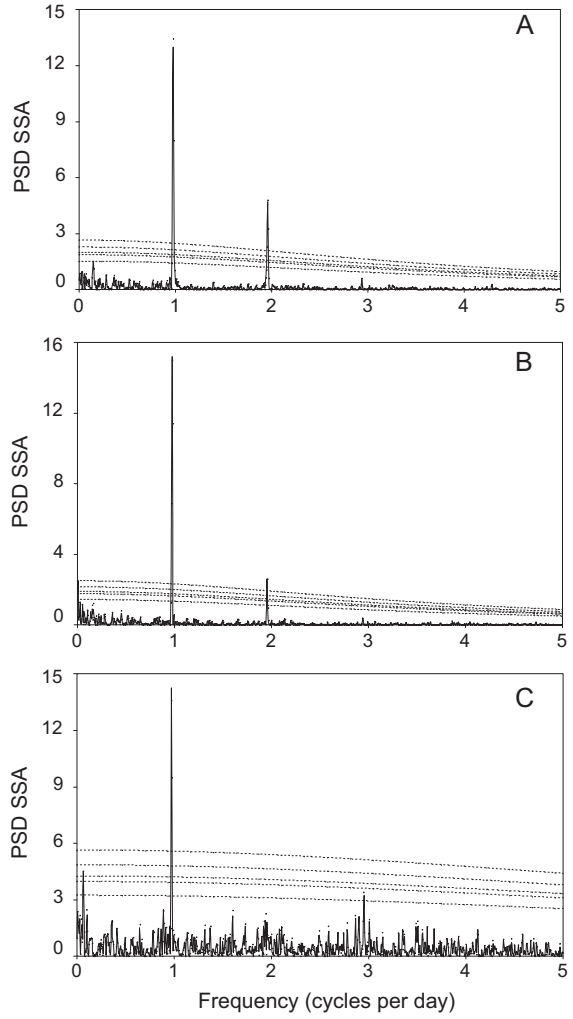

Fig. 5. Fourier power spectra of the measured E time series for 2014. A. Trout Bog; B. Crystal Bog; C. Little Rock Lake. Time series are 30 min observations smoothed using a 3.5 h centered moving average (May to November). PSD SSA, power spectral density sum squared average. CS2 Hann window. Curves indicate 50%, 90%, 95%, 99% and 99.9% significance levels (red noise model). The minor peaks at 2, 3 and 4 cycles per day are integer harmonics of the 1 d^{-1} frequency of the evaporation waveform (i.e. the daily oscillation is not a pure sine wave).

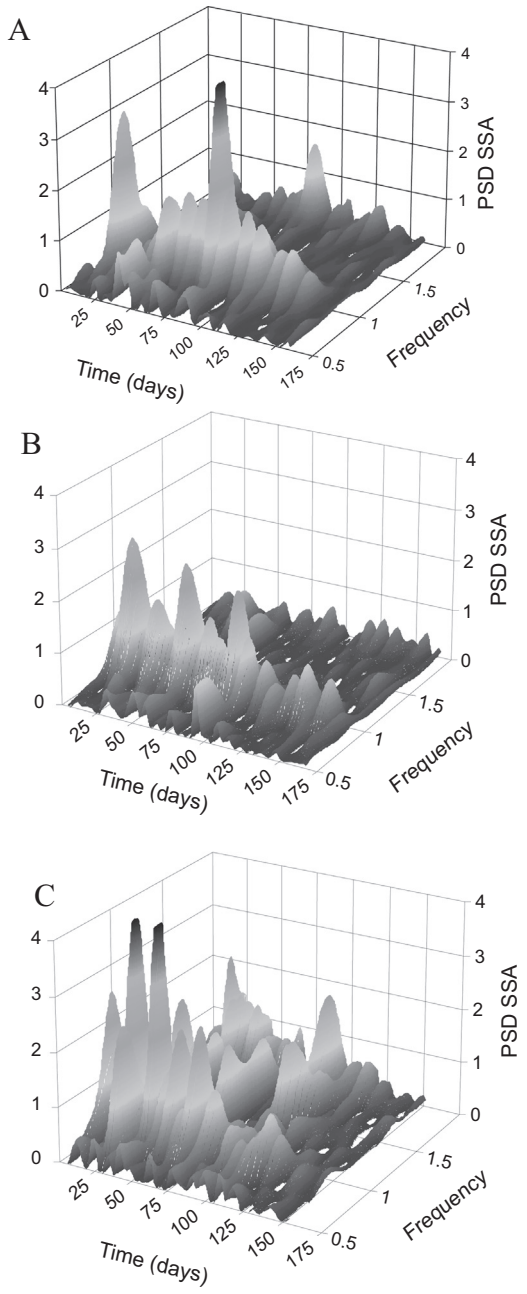

Fig. 6. Short-term Fourier transform of measured evaporation rates (3.5 h centered moving average of 30 min data) in Trout Bog (A), Crystal Bog (B) and Little Rock Lake (C) during 2014. Sequential weekly time segments (336 points) with 50% overlap; CS2 Hann window; PSD SSA, power spectral density sum squared average; frequencies <0.5 cycles per day omitted.

2.7. Deployment years

Instrumentation was deployed during the ice-free period in Trout Bog for 4 consecutive years (2012–2015). In Crystal Bog, the deployment period was 3 years (2013–2015). In Little Rock Lake, deployment was for 2 years (2014 and 2015). Ancillary climatic data were not collected during 2015, so mass transfer modeling was limited to 3 years (2012–2014).

3. Findings and significance

3.1. Sunlight absorbance and surface water temperatures

As observed by others (e.g. Williamson et al., 1996; Read and Rose, 2013), light absorption by surface water from the study lakes increased with increasing DOC concentration at all wavelengths from 200 to 750 nm (Fig. 2 top). Absorbance in the region 275–295 nm ($S_{275-295}$), indicates that the DOC in Crystal Bog and Trout Bog was dominated by non-photodegraded humic matter derived from riparian peatland (Helms et al., 2008). Because of solar energy absorbance by DOC, the temperature of near surface waters also increased with increasing DOC (Fig. 2). This relationship was observed in all four years of study (Table 2). There was a strong diel temperature cycle in all 3 lakes, and the amplitude was directly related to DOC concentration. The greater amplitude in dark water lakes was due mainly to an increase in the daily maximum temperature.

Our temperature findings are not consistent with results for a similar set of lakes in the NHLD by Houser (2006). In contrast to our results, Houser reported that epilimnetic temperatures decreased with increasing DOC. The disparity is likely due to

differences in the depth of temperature sensors and strong temperature gradients in the upper water of dark lakes. Whereas we targeted a depth of 0.1 m for our sensors, Houser's sensors were at depths of 0.5–0.7 m. Since less than 10% of the incident solar radiation penetrates to a depth of 0.5 m in high DOC lakes like Trout Bog, surface waters tend to stratify strongly during daytime (Watras et al., 2015). As a result, the upper-most water of high DOC lakes can be significantly warmer than low DOC lakes; even though the total heat content of high DOC lakes may be substantially lower because deep waters remain cold (Read and Rose, 2013).

3.2. Measured evaporation rates

Daily rates of evaporation from all of the floating E-pans increased from spring through summer and then decreased to minimum values in fall (Fig. 3). Day to day variability was high (as much as 4 mm d^{-1}), with daily rates ranging from <0 to ~7 mm d^{-1} in all three lakes. Among all lakes and years, there were 85 d when E was negative (5%). The cause of negative values remains unclear, but we suspect that it is related to uncertainties in estimating E on rainy days when E is already low. It rained on 82% of the days with negative values. Condensation at night may be a contributing factor, but published estimates of dew formation in humid northern climates suggest it would likely account for less than 0.5 mm d^{-1} (Jacobs et al., 2008).

The high day to day variability in E we observed is consistent with the findings of Lenters et al. (2005) who constructed energy balances for nearby Sparkling Lake. However, when integrated over seasonal time scales, E generally varied by <1 mm d^{-1} for a given lake. Overall, the annualized E among all 3 lakes and years averaged 2.8 mm d^{-1} with a coefficient of variation of 9% (Fig. 3 tabulation), which is similar to the long-term, average rate reported by Lenters et al. for Sparkling Lake (3.1 mm d^{-1}; CV, 25%; 1989–1998).

Despite the large day to day variability, there were statistically significant differences in measured E among the three lakes (Table 3). In all years, Trout Bog had the lowest rates of evaporation, followed by Crystal Bog and then Little Rock Lake. During summer, when evaporation was highest, the difference in daily E between the darkest and clearest lake averaged ~24% (0.8 mm d^{-1}) (Fig. 3 tabulation). When the daily difference was accumulated over the open-water period, it amounted to 15 cm in excess evaporative water loss from the clearest lake in 2015 and 6 cm in 2014 (Table 3 and Fig. 4A). Interestingly, these results run counter to the observed differences in surface temperature which was highest in the dark lake (Table 2).

This finding suggests that either there is a hidden sink for surficial heat in the darker lake, or that other environmental factors are modulating the effect of water temperature on E despite apparent similarities in hydrologic setting and micro-meteorology. One explanation is suggested by the water temperature modeling of Read and Rose (2013). Their results indicate that the relatively high surface temperature of sheltered, dark lakes increases the rate of outward radiation from the water surface; and they suggest that outward radiation was more important to balancing the energy budget in these lakes than the sum of latent and sensible heat loss. In other words, the ratio $[R_{out}/(L+H)]$ increases with increasing DOC (where R_{out} is long wave radiation leaving the lake, L is the latent heat loss and H is the sensible heat loss).

Although there were statistically significant differences in E between lakes (Table 3), daily rates of evaporation were highly correlated among lakes (Fig. 4B–D). These strong inter-lake correlations suggest a common set of local drivers. Correlations with climatic variables indicated that E was most strongly related to the vapor pressure gradient and shortwave solar radiation across all lakes and time scales (Table 4). As expected, E was negatively correlated with relative humidity; but somewhat unexpectedly, the correlation between E and wind speed (W) was weak and actually negative at longer time scales. The weak correlation with W likely reflects the sheltered settings of these lakes where wind speed rarely exceeded 1.5 m s^{-1}. As pointed out by Adams et al. (1990), at low wind speeds E is nearly insensitive to W. As suggested by Lenters et al. (2005), the negative correlation may be due to seasonal changes in wind speed, which tend to be relatively high in spring and fall (when E is low) and tend to be low in summer (when E is high) at this mid-latitude location. However, these findings do not mean that wind speed is unimportant. For example, when the free convection model (Eq. (1)) was applied to the data for Trout Bog during 2014, the residuals were correlated with wind speed. The residuals were even more strongly correlated with the product of wind speed and the vapor pressure deficit $[W(e_s - e_z)]$, which indicates the overall importance of the wind speed function and forced convection.

3.2.1. Diel cycles

At the 30 min time scale, all three lakes exhibited a strong diel evaporation cycle (Fig. 4E). Fourier spectrum analysis confirmed a

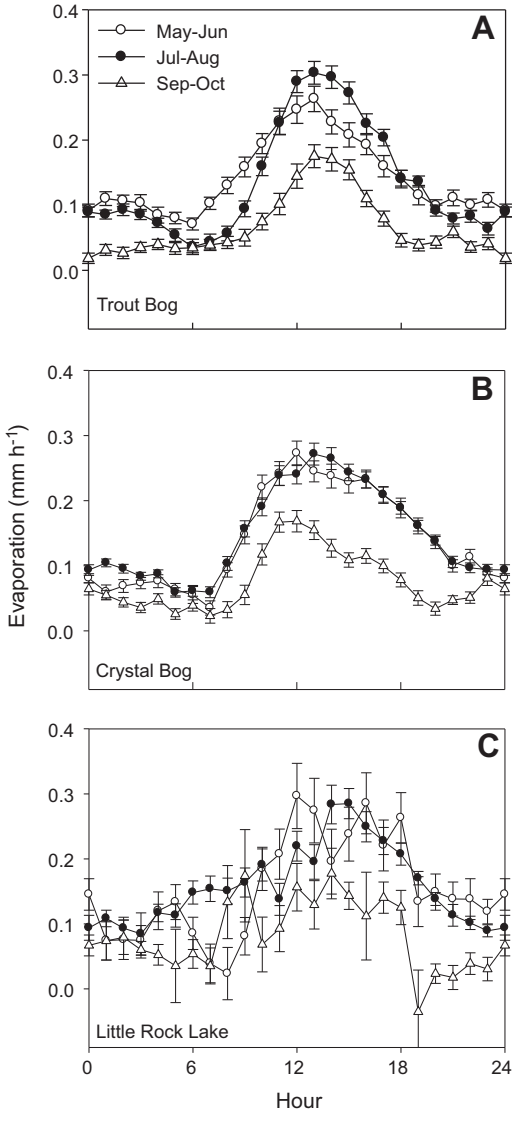

Fig. 7. Diel cycles of measured evaporation in 2014. Data are binned hourly means (±SE) during spring, summer or fall.

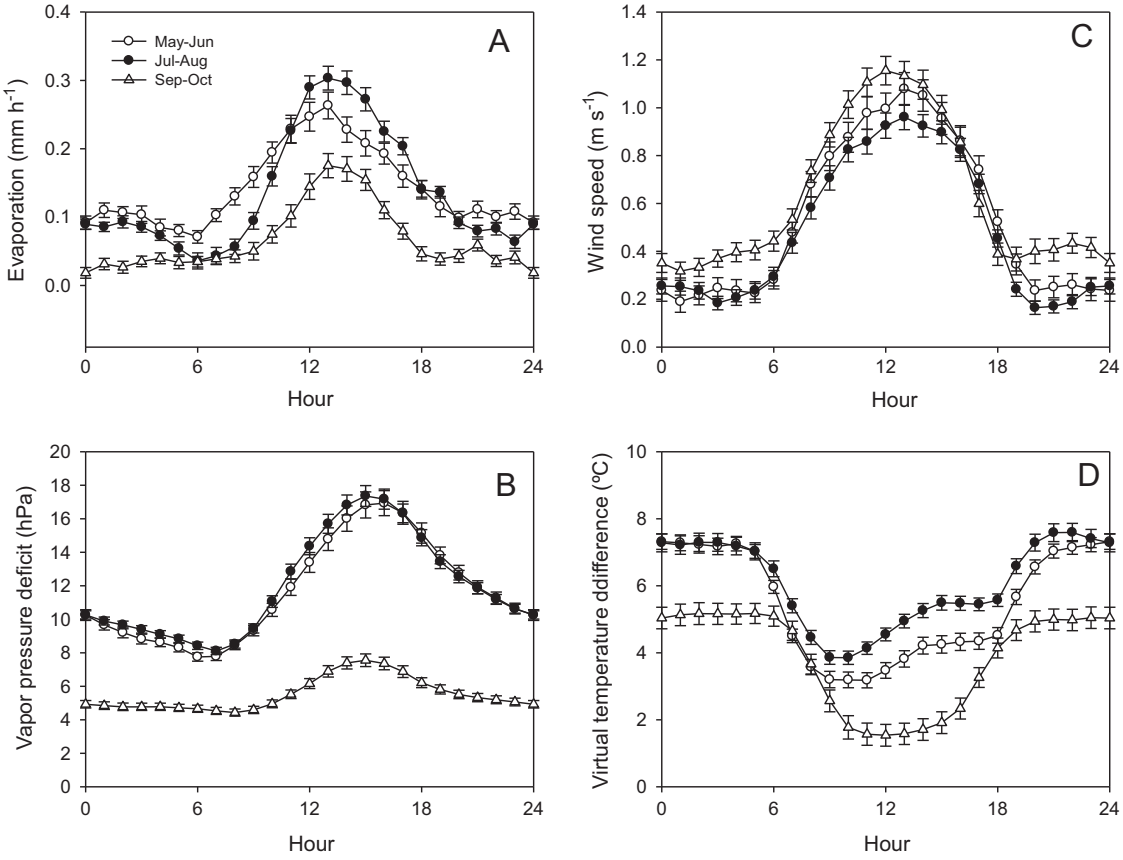

Fig. 8. Diel cycles of measured evaporation, vapor pressure deficit, wind speed and virtual temperature difference for Trout Bog, 2014. Data are binned hourly means (±SE) during spring, summer or fall.

dominant periodicity of one cycle per day in these evaporation time series (Fig. 5). The strength of the diel cycle varied from week to week in all three lakes, and the daily signal became weaker as fall progressed (Fig. 6). Binning the 30 min data into hourly time slots across all days showed that evaporation rates began to rise near dawn, peaked near solar noon and then declined to minima that were relatively constant until the following morning (Fig. 7). The amplitude of the diel cycle varied among seasons, years and lakes; but the phase was fairly constant. The highest rates and greatest amplitudes were observed during summer (July and August). Over the course of an average summer day, evaporation rates varied from about 0.05 mm h^{-1} at night to about 0.3 mm h^{-1} near noon.

Strong diel cycles were also evident in time series for three climatic variables that drive mass transfer models: the vapor pressure gradient, wind speed and the virtual temperature difference (Fig. 8, Suppl. Fig. 1). All of these diel cycles are ultimately governed by the solar cycle; and with one exception, their seasonality reflected seasonal changes in solar radiation (Fig. 9). The exception was the diel cycle of wind speed (Fig. 8C), which as noted above tends to be higher in spring and fall than in summer. The apparent contradiction between the seasonality of diel E and W may be resolved by coupling hourly wind speed with hourly changes in the vapor pressure gradient (see below).

Time lags between the daily oscillation of E and these variables suggest some lake-specific patterns (Table 5). The daily solar cycle generally preceded the daily cycle of E by 2–3 h, meaning, unsurprisingly, that the sun rose well before surface waters began to evaporate more strongly. Interestingly, the lag between E and SSR increased with decreasing DOC, indicating that the darker lakes begin to evaporate earlier in the morning than clearer lakes. It would seem that this early start might be related to the faster warming of surface waters in the darker lakes, consistent with the absorbance spectra (Fig. 2) in spite of their lower E overall. Close inspection of the temperature data in Fig. 2 indicates that Trout Bog does indeed begin to warm each day before the other two lakes. Wind speed also picked up in the morning before E began to rise; and again a shorter lag for the darker lakes points to the earlier rise in E. For all 3 lakes, the virtual temperature difference between water and air was almost completely out of phase with the evaporation cycle (lag approaching 12 h), reflecting the fact that air warmed faster than water in the early morning hours and declined faster in the evening (data not shown).

Inter-lake differences in the daily oscillations of wind speed (W) and the vapor pressure gradient ($e_s - e_z$) suggest a second explanatory mechanism potentially underlying the unexpected relationship between DOC, surface T and E (Fig. 10). The critical variable appears to be the wind speed function (Fig. 10B), represented by the product $[W(e_s - e_z)]$. Both Little Rock Lake and Crystal Bog are somewhat less sheltered than Trout Bog (Hanson et al., 2014); and consequent differences in $[W(e_s\, e_z)]$ show a clear separation of the three lakes into two groups that are somewhat consistent with the ranking of evaporation rates (LRL ≈ CB > TB). This separation is not evident in the vapor pressure gradient alone (Fig. 10A) or the virtual temperature difference (Fig. 10C). Thus, even though W was a weak correlate of E overall, it may help to

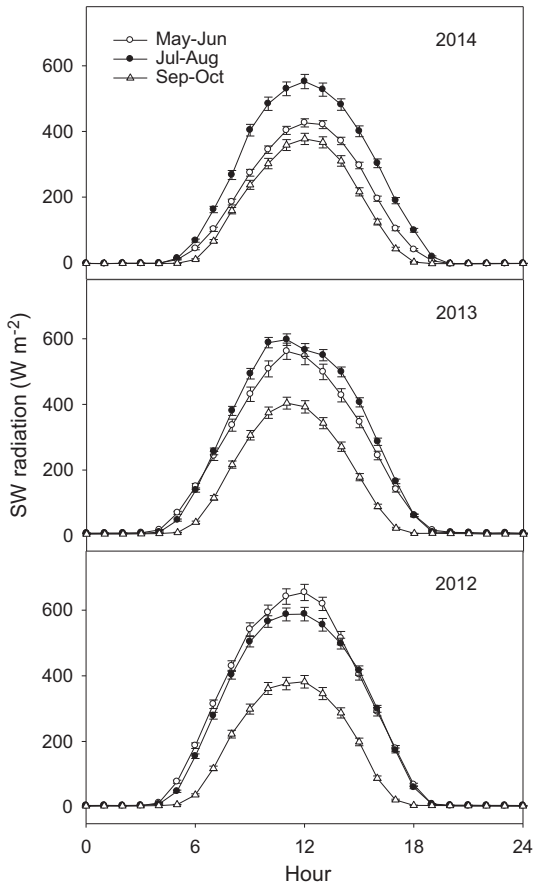

Fig. 9. Diel cycle of short wave solar radiation (SSR) in the study area for each of three years. Data are binned means ± SE for each hour of the day during spring, summer and fall seasons.

explain the inter-lake differences in measured rates of evaporation, especially when coupled with the disproportionate increase in $[R_{out}/(L+H)]$ with DOC mentioned above.

3.3. Modeled evaporation rates

At least 5 prior studies have evaluated the efficacy of various equations in determining evaporation rates from northern temperate/boreal lakes (Rasmussen et al., 1995; Winter et al., 1995; Singh and Xu, 1997; Rosenberry et al., 2004, 2007). Each study designated a standard against which performance was judged. In our study, the standard was measured evaporation from the floating E-pans. One strength of this approach is that E is measured directly; a weakness is that measurement error is unquantified because only one pan was deployed in each lake (a limitation that is also common to most modeling approaches). With this constraint, comparisons among the mass transfer models indicate that the equations with defined wind speed functions (Eqs. (3) and (4)) provided reasonably good fits to measured rates of evaporation at daily time scales (Fig. 11, Suppl. Fig. 2). Even though wind speeds were very low on all lakes (<1.5 m s^{-1}), the free convection model performed poorly and substantially underestimated E in all cases (Fig. 11C, F, I; Suppl. Fig. 2C, F, I). As observed for rates measured in the E-pans, the high DOC lake (dark) also had the lowest modeled rates of evaporation (Table 3).

Not surprisingly, running models 2 and 3 with fitted constants rather than the original published constants yielded stronger relationships to measured E across all lakes and years (Table 6). Coefficient "*a*" applies to the free convection term; and as indicated in Table 6, the fitted value was similar to the published value of 2.7. However, the fitted value of coefficient "*b*" was higher by a factor of ~2 than the published value (Table 6). Since coefficient "*b*" amplifies the wind speed function, this result implies that the original models underestimate the importance of wind speed on these small lakes. This conclusion is consistent with the plots in Fig. 11 and Suppl. Fig. 2, which indicate that the models are underestimating measured E. When fitted constants are applied, the models still underestimate measured E but considerably less so (Table 6).

The results of our measured-to-modeled comparisons are similar to those reported in other studies of small lakes using different performance criteria. Rasmussen et al. (1995) reported regression coefficients (r^2) that ranged from 0.67 to 0.91 when 7 mass transfer models were applied to 9 Minnesota lakes. For the Minnesota lakes, measured water temperature at 1 m depth was used as the performance standard, and Eq. (3) was considered the best fitting model. Rosenberry et al. (2007) compared Eq. (3) to an energy balance model for a small New Hampshire lake and reported a slope close to 1 but a regression coefficient (r^2) of only 0.60 when the published constants were applied (cf. Table 6). In a study of a small Australian reservoir, McGloin et al. (2014) compared the performance of 5 mass transfer models against an eddy covariance model and reported slopes that ranged from 0.74 to 1.02 and correlation coefficients (r^2) that ranged from 0.83 to 0.86.

Given the different standards against which model performance has been evaluated, it is hard to point conclusively to a "best method" among the various approaches and formulations available. Nonetheless, reasonably good agreement among methods suggests that mass transfer models may be aptly suited for small lakes, especially when cost constraints apply. For our 3 study lakes, the models were able to capture both temporal and inter-lake differences observed with the direct E-pan measurements.

3.4. Water budgets

The intensive hydrologic data collected on Trout Bog and Crystal Bog allowed us to construct highly resolved water budgets (daily time steps) for the open-water season in each of 4 years (Fig. 12). The budgets indicate that evaporation was always the dominant loss process, and that lake stage fluctuated as the balance between P and E varied with precipitation events and intervening periods of dryout. Net seepage was generally away from both lakes into the surrounding peatland (groundwater recharge), but there were several episodes of flow reversal associated with rain events due to the high specific yield of peat. An anomalously large event at the end of 2012 was associated with an intense storm and a sharp spike in lake stage, especially for Trout Bog. The upland adjacent to the Trout Bog had been logged shortly before this event, and water table wells deployed in the peatland showed a similar, short-duration rise in water levels (data not shown).

Since high-frequency data for lake stage was not collected in Little Rock Lake, and since E was measured only for two years, highly resolved water budgets could not be constructed and compared to those for the two bogs. However, prior water budgets for the years 1984–1990 indicate similarities with the other 2 lakes (Rose, 1993). During those 7 years, water input to Little Rock Lake was dominated by precipitation (~99%) and water loss was dominated by evaporation (~67%) with out-seepage to the underlying aquifer accounting for the remainder. Exchange with the local

Table 5
Time lags between the diel cycle of E and the diel cycles of climate variables during 2014 (cf. Figs. 7 and 8). Lags were calculated using: lag = $(\cos^{-1} r)\cdot(24/2\pi)$, where r is the linear correlation coefficient. A positive lag means that E precedes the correlate in time. SSR, shortwave solar radiation; $(e_{sw} - e_a)$, vapor pressure deficit; (Tvs–Tva), virtual temperature difference; W, wind speed.

Correlate	Lake	Season	r	Lag (h)
SSR	Trout Bog	Spring	0.91	−1.6
		Summer	0.79	−2.5
		Fall	0.82	−2.3
	Crystal Bog	Spring	0.79	−2.5
		Summer	0.82	−2.3
		Fall	0.82	−2.3
	Little Rock Lake	Spring	0.55	−3.8
		Summer	0.70	−3.0
		Fall	0.66	−3.3
$(e_{sw} - e_a)$	Trout Bog	Spring	0.67	3.2
		Summer	0.87	1.9
		Fall	0.81	2.4
	Crystal Bog	Spring	0.80	2.4
		Summer	0.86	2.0
		Fall	0.81	2.4
	Little Rock Lake	Spring	0.86	2.1
		Summer	0.88	1.9
		Fall	0.57	3.7
$(\text{Tvs} - \text{Tva})^{1/3}$	Trout Bog	Spring	−0.81	−9.6
		Summer	−0.55	−8.2
		Fall	−0.87	−10.1
	Crystal Bog	Spring	−0.74	−9.2
		Summer	−0.72	−9.1
		Fall	−0.85	−9.8
	Little Rock Lake	Spring	−0.66	−8.8
		Summer	−0.78	−9.4
		Fall	−0.75	−9.3
W	Trout Bog	Spring	0.95	−1.2
		Summer	0.85	−2.1
		Fall	0.87	−2.0
	Crystal Bog	Spring	0.83	−2.3
		Summer	0.87	−2.0
		Fall	0.82	−2.3
	Little Rock Lake	Spring	0.58	−3.6
		Summer	0.78	−2.6
		Fall	0.69	−3.1

aquifer was transient, but discharge from groundwater to the lake only accounted for ~1% of inputs on average. As observed for the bog lakes, annual changes in lake stage were related to the balance between P and E, with E/P varying from about 0.6 to 0.9 among years when water levels either rose or declined.

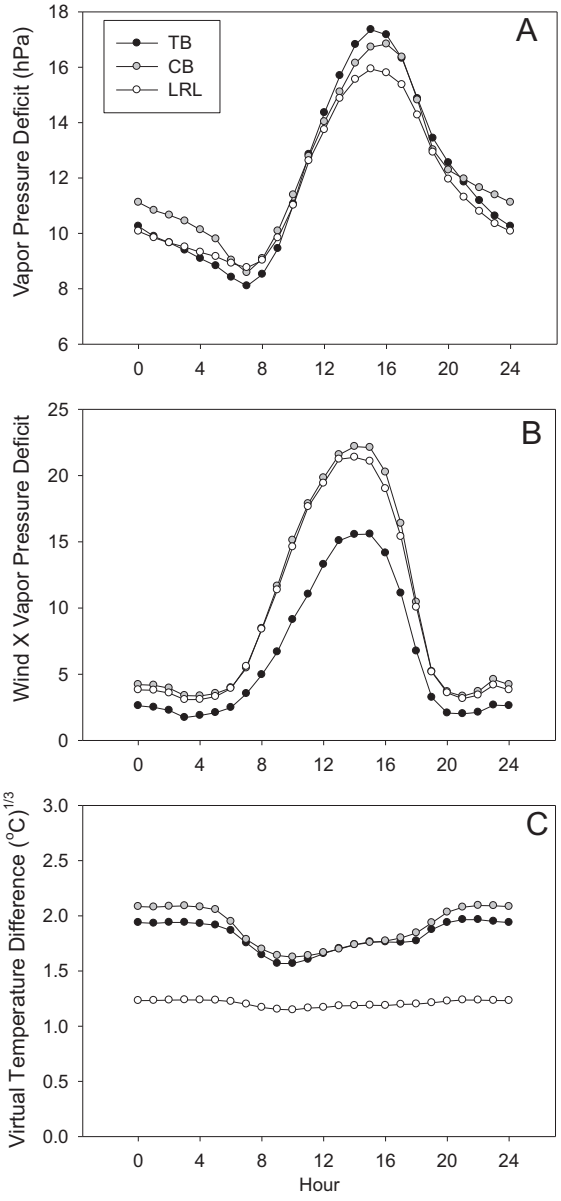

Fig. 10. Micro-meteorological components of evaporation, average daily cycles for summer during 2014 in Trout Bog (TB), Crystal Bog (CB) and Little Rock Lake (LRL). Here the virtual temperature difference is reported as the cube root, as in Eq. (3).

4. Conclusions and implications

Our findings confirm that DOC enhances surface water temperature, but the effect of DOC does not necessarily translate directly to a higher evaporation rate. One possible reason is that high DOC lakes may lose disproportionately more energy via radiant outflux than low DOC lakes (Read and Rose, 2013). A second reason is that wind sheltering by riparian forest and bluff can have a significant impact on E, even differentiating among very small lakes where wind shadows are large and wind speeds are low (<1.5 m s^{-1}). For management practices, the latter finding implies the importance of maintaining riparian forest cover, especially by tall, long-lived tree species. As Markfort et al. (2010) have shown, the wind shadow may extend 40–60 h from the shoreline, where h is the canopy height. For mature riparian tree stands in the Great Lakes region of North America, this corresponds to sheltered lengths of 400–900 m, a significant distance even for medium size lakes. The thickness of riparian stands is also an important factor since it determines the amount of wind that breaks though the tree line.

Our results also indicate that although annually averaged rates of evaporation are remarkably similar among small lakes in this region (~3 mm d^{-1}), apparently minor differences in daily E among lakes and years can have significant, cumulative effect on water budgets (cf. Rose, 1993; Hanrahan et al., 2010; Watras et al., 2014a). The cumulative effect can be seen on an annual time scale in Fig. 4A. Thus, even modest changes in future climatic conditions which shift the balance between P and E from the historical mean would be expected to gradually impact water levels over the long term.

Finally, we conclude that floating E-pans can be useful tools for estimating E on small lakes, providing empirical data useful for

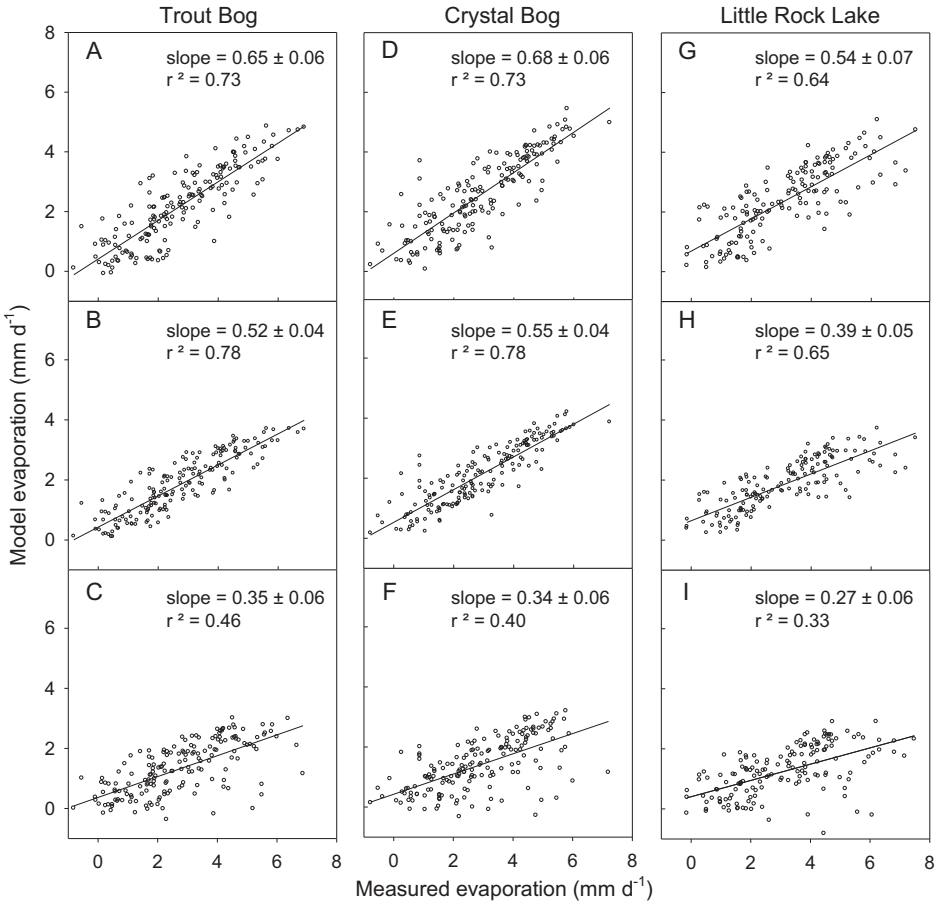

Fig. 11. Measured versus modeled evaporation for the study lakes during 2014. Panels A, D, G: Eq. (3). Panels B, E, H: Eq. (4). Panels C, F, I: Eq. (1). Lines indicate linear regression.

Table 6
Parameter estimates for mass transfer models fitted to measured evaporation rates (E-pan data). Slope and r^2 from linear regression of measured E on modeled E with fitted constants (both mm d^{-1}). Published constants from original works.

Lake	Year	Mass transfer model							
		Ryan–Harleman (Eq. (3))				Adams–Helfrich (Eq. (4))			
		a	*b*	Slope	r^2	*a*	*b*	Slope	r^2
Trout Bog	2014	2.44	5.91	0.80 ± 0.08	0.71	2.58	12.03	0.79 ± 0.06	0.78
	2013	2.24	6.01	0.71 ± 0.08	0.66	2.27	12.00	0.71 ± 0.07	0.70
	2012	2.47	4.03	0.71 ± 0.06	0.70	2.78	8.76	0.71 ± 0.06	0.76
Crystal Bog	2014	2.00	5.47	0.77 ± 0.07	0.76	2.24	10.87	0.76 ± 0.06	0.81
	2013	2.13	5.06	0.85 ± 0.07	0.79	2.26	10.45	0.83 ± 0.05	0.84
Little Rock	2014	2.78	4.90	0.66 ± 0.08	0.64	3.11	11.14	0.63 ± 0.07	0.68
Mean ± SD		2.3 ± 0.3	5.2 ± 0.7	0.75 ± 0.07	0.71 ± 0.06	2.6 ± 0.4	10.9 ± 1.2	0.74 ± 0.07	0.76 ± 0.06
Published constant		2.7	3.1			2.7	5.1		

model calibration and validation (cf. Masoner and Stannard, 2010; Masoner et al., 2008). In our study, there was reasonably good agreement between directly measured E and the output of several mass transfer models, all of which have relatively modest data requirements. Upscaling to medium size lakes will require more rugged E-pan designs and a re-assessment of modeling approaches.

Acknowledgements

Support was provided by the Wisconsin Department of Natural Resources and by the US National Science Foundation (Grant Nos. DEB-0822700; DEB-0941510; DBI-0639229). We thank Jordan Read and Tim Kratz for helpful discussions and insights. We also thank three anonymous reviewers for insightful comments and

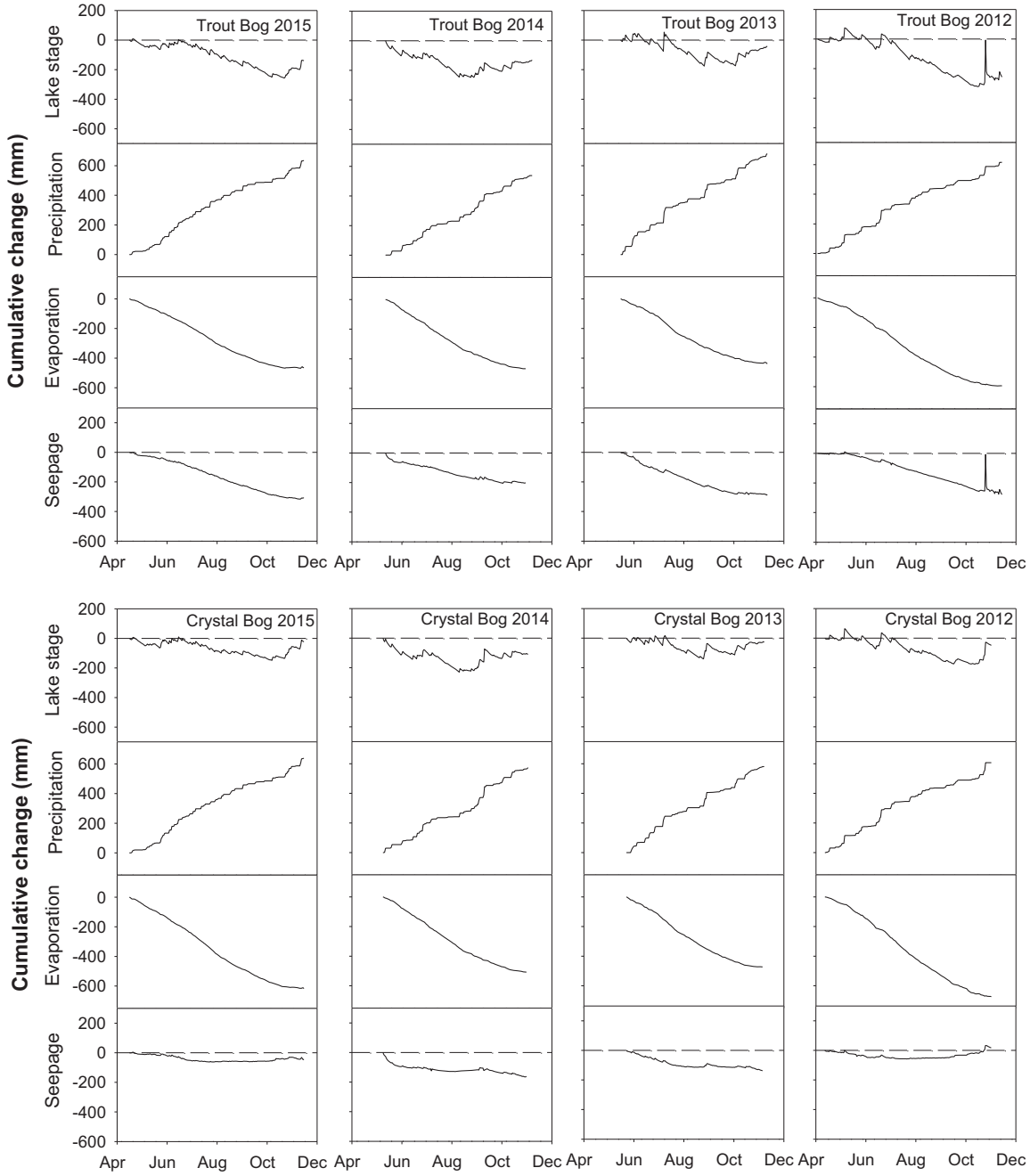

Fig. 12. Elements of the water budgets for Trout Bog and Crystal Bog, 2012–2015, constructed using daily data for lake stage, precipitation and evaporation (seepage as residual term).

Tim McVicar for editorial suggestions. This is a joint contribution from the Fishery and Aquatic Science Section, WI DNR, and the Trout Lake Station, Center for Limnology, University of Wisconsin-Madison.

Appendix A. Supplementary data

Supplementary data associated with this article can be found, in the online version, at http://dx.doi.org/10.1016/j.jhydrol.2016.06.002.

References

Adams, E.E., Cosler, D.J., Helfrich, K.R., 1990. Evaporation from heated water bodies: predicting combined forced plus free convection. Water Res. Res. 26 (3), 425–435.

Adams, E.E., Helfrich, K.R., 1982. Analysis of Evaporation Measurements Taken from June 16-July 15, 1981 at the Heated Ponds at the National Geothermal Test Facility at East Mesa, CA. Energy Lab Report. MIT, Cambridge, MA.

Austin, J.A., Colman, S.M., 2007. Lake superior summer water temperatures are increasing more rapidly than regional air temperatures: a positive ice-albedo feedback. Geophys. Res. Lett. 34, L06604. http://dx.doi.org/10.1029/2006GL029021.

Attig, J.W., 1985. Pleistocene geology of Vilas County, Wisconsin. Wisconsin Geological and Natural History Information Circular, vol. 50, p. 32.

Brutseart, W., 1982. Evaporation into the Atmosphere: Theory, History and Applications. Reidel Publishing, Dordrecht, NDL.

Brutsaert, W., Parlange, M.B., 1998. Hydrologic cycle explains the evaporation paradox. Nature 396, 30.

Downing, J.A., Prairie, Y.T., Cole, J.J., Duarte, C.M., Tranvik, L.J., Striegl, R.G., et al., 2006. The global abundance and size distribution of lakes, ponds, and impoundments. Limnol. Oceanogr. 51, 2388–2397.

Hanrahan, J.L., Kravtsov, S.V., Roebber, P.J., 2010. Connecting past and present climate variability to the water levels of Lakes Michigan and Huron. Geophys. Res. Lett. 37 (1). http://dx.doi.org/10.1029/2009gl041707.

Hanrahan, J., Roebber, P., Kravtsov, S., 2014. Attribution of decadal-scale lake-level trends in the Michigan-Huron system. Water 6 (8), 2278–2299.
Hanson, P.C. et al., 2014. Quantifying lake allochthonous organic carbon budgets using a simple equilibrium model. Limnol. Oceanogr. 59 (1), 167–181.
Harbeck, G.E., 1962. A Practical Field Technique for Measuring Reservoir Evaporation Utilizing Mass-transfer Theory. U.S. Geological Survey Prof. Paper 272E.
Held, I.M., Soden, B.J., 2006. Robust responses of the hydrological cycle to global warming. J. Climate 19, 5686–5699.
Helms, J.R., Stubbins, A., Ritchie, J.D., Minor, E.C., Kieber, D.J., Mopper, K., 2008. Absorption spectral slopes, and slope ratios as indicators of molecular weight, source, and photobleaching of chromophoric dissolved organic matter. Limnol. Oceanogr. 53, 955–969.
Houser, J.N., 2006. Water color affects the stratification, surface temperature, heat content, and mean epilimnetic irradiance of small lakes. Can. J. Fish. Aquat. Sci. 63 (11), 2447–2455.
INW, Inc., 1995. Digitally-temperature-compensated Strain-gauge Pressure Measuring Apparatus: US Patent No. 5460049. <https://www.google.com/patents/US5460049>.
Jacobs, A.F.G., Heusinkveld, B.G., Berkowicz, S.M., 2008. Passive dew collection in a grassland area. The Netherlands. Atmos. Res. 87, 377–385.
Lenters, J.D., Kratz, T.K., Bowser, C.J., 2005. Effects of climate variability on lake evaporation: results from a long-term energy budget study of Sparkling Lake, northern Wisconsin (USA). J. Hydrol. 308, 168–195.
Magnuson, J.J. et al., 2000. Historical trends in lake and river ice cover in the Northern Hemisphere. Science 289 (5485), 1743–1746. http://dx.doi.org/10.1126/science.289.5485.1743.
Magnuson, J.J., Kratz, T.K., Benson, B.J. (Eds.), 2006. Long-term Dynamics of Lakes in the Landscape. Oxford University Press, p. 400.
Markfort, C.D. et al., 2010. Wind sheltering of a lake by a tree canopy or bluff topography. Water. Resources Res. 46, W03530, doi: 10.1029/2009WR007759.
Masoner, J.R., Stannard, D.I., 2010. A comparison of methods for estimating open-water evaporation from small wetlands. Wetlands 30, 513–524.
Masoner, J.R., Stannard, D.I., Christenson, S.C., 2008. Differences in evaporation from a floating pan and a class A pan on land. J. Am. Water Res. Assoc. 44, 552–561.
McDonald, C.P., Rover, J.A., Stets, E.G., Striegl, R.G., 2012. The regional abundance and size distribution of lakes and reservoirs in the United States and implications for estimates of global lake extent. Limnol. Oceanogr. 57, 1–12.
McGloin, R., McGowen, H., McJannet, D., Burn, S., 2014. Modelling sub-daily latent heat fluxes from a small reservoir. J. Hydrol. 519, 2301–2311.
McVicar, T.R., Roderick, M.L., et al., 2012. Global review and synthesis of trends in observed terrestrial near-surface wind speeds: implications for evaporation. J. Hydrol. 416–417, 182–205.
Melillo, J.M., Richmond, T.C., Yohe, G.W. (Eds.), 2014. Climate Change Impacts in the United States: The Third National Climate Assessment. U.S. Global Change Research Program, p. 841. http://dx.doi.org/10.7930/J0Z31WJ2.
Mendoza-Sanchez, I., Phanikumar a, M.S., Niu, J., Masoner, J.R., Cozzarelli, I.M., McGuire, J.T., 2013. Quantifying wetland–aquifer interactions in a humid subtropical climate region: an integrated approach. J. Hydrol. 498, 237–253.
Mishra, V., Cherkauer, K.A., Bowling, L.C., 2011. Changing thermal dynamics of lakes in the Great Lakes region: role of ice cover feedbacks. Global Planet. Change 75 (3–4), 155–172. http://dx.doi.org/10.1016/j.gloplacha.2010.11.003.
O'Reilly, C.M. et al., 2015. Rapid and highly variable warming of lake surface waters around the globe. Geophys. Res. Lett. 42. http://dx.doi.org/10.1002/2015GL066235.
Rasmussen, A.H., Hondzo, M., Stefan, H.G., 1995. A test of several evaporation equations for water temperature simulations in lakes. Water Res. Bull. 31 (6), 1023–1028.
Read, J.S., Rose, K.C., 2013. Physical responses of small temperate lakes to variation in dissolved organic carbon concentrations. Limnol. Oceanogr. 58 (3), 921–931.
Roderick, M.L., Sun, F., Lim, W.H., Farquhar, G.D., 2014. A general framework for understanding the response of the water cycle to global warming over land and ocean. Hydrol. Earth Syst. Sci. 18, 1575–1589. http://dx.doi.org/10.5194/hess-18-1575-2014.
Rose, W.J., 1993. Hydrology of Little Rock Lake in Vilas County, North-central Wisconsin. U.S. Geological Survey Water-Resources Investigations Report 93-4139, 22p.
Rosenberry, D.O., Winter, T.C., Buso, D.C., Likens, G.E., 2007. Comparison of 15 evaporation methods applied to a small mountain lakes in the northeastern USA. J. Hydrol. 340, 149–166.
Rosenberry, D.O., Stannard, D.I., Winter, Martinez, M.L., 2004. Comparison of 13 equations for determining evapotranspiration from a prarie wetland, Cotonwood Lake area, North Dakota, USA. Wetlands 24, 483–497.
Ryan, P.J., Harleman, D.R.F., 1973. An Analytical and Experimental Study of Transient Cooling Pond Behavior Tech. Rpt. 161. R.M. Parsons Laboratory, MIT, Cambridge, MA.
Ryan, P.J., Harleman, D.R.F., Stolzenbach, K.D., 1974. Surface heat loss from cooling ponds. Water Res. Res. 10 (5), 930–938.
Sherwood, S., Fu, Q., 2014. A drier future? Science 243, 737–739.
Singh, V.P., Xu, C.Y., 1997. Evaluation and generalization of 13 mass-transfer equations for determining free water evaporation. Hydrol. Process. 11, 311–323.
Watras, C.J., Read, J.S., Holman, K.D., Liu, Z., Song, Y.-Y., Watras, A.J., Morgan, S., Stanley, E.H., 2014a. Decadal oscillation of lakes and aquifers in the upper Great Lakes region of North America: hydroclimatic implications. Geophys. Res. Lett. 41, 456–462. http://dx.doi.org/10.1002/2013GL058679.
Watras, C.J., Morrow, M., Morrison, K., Scannell, S., Yaziciaglu, S., Read, J.S., Hu, Y.-H., Hanson, P.C., Kratz, T., 2014b. Evaluation of wireless sensor networks (WSNs) for remote wetland monitoring: design and initial results. Environ. Monit. Assess. 186, 919–934.
Watras, C.J., Morrison, K.A., Crawford, J.T., McDonald, C.P., Oliver, S.K., Hanson, P.C., 2015. Diel cycles in the fluorescence of dissolved organic matter in dystrophic Wisconsin seepage lakes: implications for carbon turnover. Limnol. Oceanogr. 60, 482–496. http://dx.doi.org/10.1002/lno.10026.
Wild, M., 2012. Enlightening global dimming and brightening. Bull. Am. Meteorol. Soc. 93 (1), 27–37.
Wild, M., Liepert, B., 2010. The earth radiation balance as driver of the global hydrological cycle. Environ. Res. Lett. 5, 1–8.
Williamson, C.E., Stemberger, R.S., Morris, D.P., et al., 1996. Ultraviolet radiation in North American lakes: attenuation estimates from DOC measurements and implications for plankton communities. Limnol. Oceanogr. 41 (5), 1024–1034.
Winter, T.C., Rosenberry, D.O., Sturrock, A.M., 1995. Evaluation of 11 equations for determining evaporation for a small lake in northcentral United States. Water Resources Res. 31, 983–993.